Modular Approach toward Bioactive Fiber Meshes Carrying Oligosaccharides

ARTICLE *in* MACROMOLECULES · NOVEMBER 2010

Impact Factor: 5.8 · DOI: 10.1021/ma101607a · Source: OAI

Macromolecules
ARTICLE

Macromolecules **2010**, *43*, 9239–9247 **9239**
DOI: 10.1021/ma101607a

Modular Approach toward Bioactive Fiber Meshes Carrying Oligosaccharides

Rafael Gentsch,[†,‡] Falko Pippig,[∥] Katja Nilles,[⊥] Patrick Theato,[⊥] Raghavendra Kikkeri,[§] Maha Maglinao,[§] Bernd Lepenies,[§] Peter H. Seeberger,[§,#] and Hans G. Börner*[,†]

[†]*Department of Chemistry, Laboratory of Organic Synthesis of Functional Systems, Humboldt-Universität zu Berlin, D-12489 Berlin, Germany,* [‡]*Department of Colloid Chemistry, Max Planck Institute of Colloids and Interfaces, Research Campus Golm, 14424 Potsdam, Germany,* [§]*Department of Biomolecular Systems, Max Planck Institute of Colloids and Interfaces, Research Campus Golm, 14424 Potsdam, Germany,* [∥]*Fraunhofer Institute for Applied Polymer Research, 14476 Potsdam, Germany,* [⊥]*Institute of Organic Chemistry, Johannes Gutenberg University Mainz, Düsbergweg 10-14 55099 Mainz, Germany, and* [#]*Institute of Chemistry and Biochemistry, Department of Biology, Chemistry and Pharmacy, Free University Berlin, Arnimallee 22, 14195 Berlin, Germany*

Received July 16, 2010; Revised Manuscript Received September 23, 2010

ABSTRACT: A modular strategy toward (bio)functional nanofiber meshes by electrospinning is described. In contrast to commonly established, multistep protocols or complex spinning setups, a straightforward single-step procedure is investigated to obtain polymer nanofibers with pentafluorophenyl (Pfp)-activated esters on the surface. The aim was to electrospin, for the first time, poly(pentafluorophenyl methacrylate) (PPfpMA) and PPfpMA/poly(ε-caprolactone) (PCL) blends, resulting in reactive nanofibers with fiber surfaces that can be functionalized with suitable bioactive entities. While PPfpMA fibers are brittle the spinning of PCL/PPfpMA blends leads to improved mechanical stability of the obtained fabrics. The effective introduction of surface functionalities onto the fibers was proven by both model compounds and bioactive monosaccharides. The Pfp-activated esters are enriched at the fiber surfaces and react cleanly with nucleophiles such as 2-aminoethanol, aminofluorescein, or amino-functionalized monosaccharides to generate a robust amide anchor. The attachment of functional entities releases a Pfp group that allows for monitoring of the functionalization reaction with UV/vis spectroscopy. X-ray photoelectron spectroscopy (XPS) and contact angle measurements indicate effective introduction of functionalities to the fiber surfaces, and fluorescence microscopy suggests a homogeneous distribution of amino functional fluorescence markers on the meshes. The bioavailability of the introduced carbohydrates is shown by macrophage stimulation experiments using PCL/PPfpMA fiber meshes, which are functionalized with 2-aminoethyl-α-D-mannopyranoside or β-D-galactopyranoside. Meshes functionalized with mannose specifically enhance the cytokine production of macrophages when costimulated with lipopolysaccharides compared to galactose- or aminoethanol-functionalized PCL/PPfpMA fiber mat controls.

Introduction

Designing and producing three-dimensional (3D) polymer materials with integrated biological activity have been identified as key issues that enable progress in several fields of biomedicine, ranging from tissue engineering to implants to biohost systems.[1−5] The establishment of effective cell−material interfaces requires the construction of materials that mimic the native biological microenvironment of cells regarding not only structural but also functional aspects.[6] Biofunctional polymer nanofiber meshes produced via electrospinning have been intensively investigated.[7] Electrospinning proved to be highly attractive due to the simplicity and versatility of the method.[8,9] The resulting nonwovens exhibit adjustable fiber diameters that can match the order of magnitude of native collagen fibers as major constituents of the extracellular matrix (ECM).[10] In addition, an inherently interconnected pore system, large active surface areas, an adjustable fiber orientation, and accessibile of hierarchical fiber constructs are benefits of these fabricated meshes.[9,11,12] The positive effects of polymer nanofiber meshes have been demonstrated for certain cell lines as adhesion, proliferation, migration, and differentiation of those cells on nanofiber scaffolds are promoted however in some cases reduced.[13−16] These effects are not surprising as cells are shown to be highly sensitive on topographies within 5 nm to 10 μm.[17−19]

Beyond topological- and mechano-signaling of polymer fibers, the biochemical functionalization of the fiber surfaces is ultimately important to establish active material interactions with biological systems.[7,20] Existing electrospin strategies to obtain nanofiber meshes with biomolecules on their surfaces can be subdivided into two major approaches: (i) direct spinning, where the functional biomolecules or blends of these with synthetic polymers are spun,[21−24] and (ii) postfunctionalization strategies, which involve the spinning of a mesh-forming polymer and subsequent introduction of functional biomolecules onto the mesh surfaces.[25,26]

Direct spinning of complex functional biomolecules is often not feasible, very costly, or highly elaborated spin setups such as coaxial electrospinning are required.[23] The electrospinning of blends composed of the biomolecules and easy spinnable synthetic polymers like poly(ethylene oxide) (PEO) or poly(ε-caprolactone) (PCL) is more commonly applied.[22,27] This approach, however, is often limited by a reduced miscibility of the fiber forming polymer and biomolecules as well as by an inherent tendency of complex biomolecules to denature during the spinning process. Despite the fact that some physical phenomena have

*To whom correspondence should be addressed: e-mail h.boerner@hu-berlin.de; Ph +49 (0) 30-2093 7348; Fax +49 (0) 30 2093-7266.

Published on Web 10/21/2010

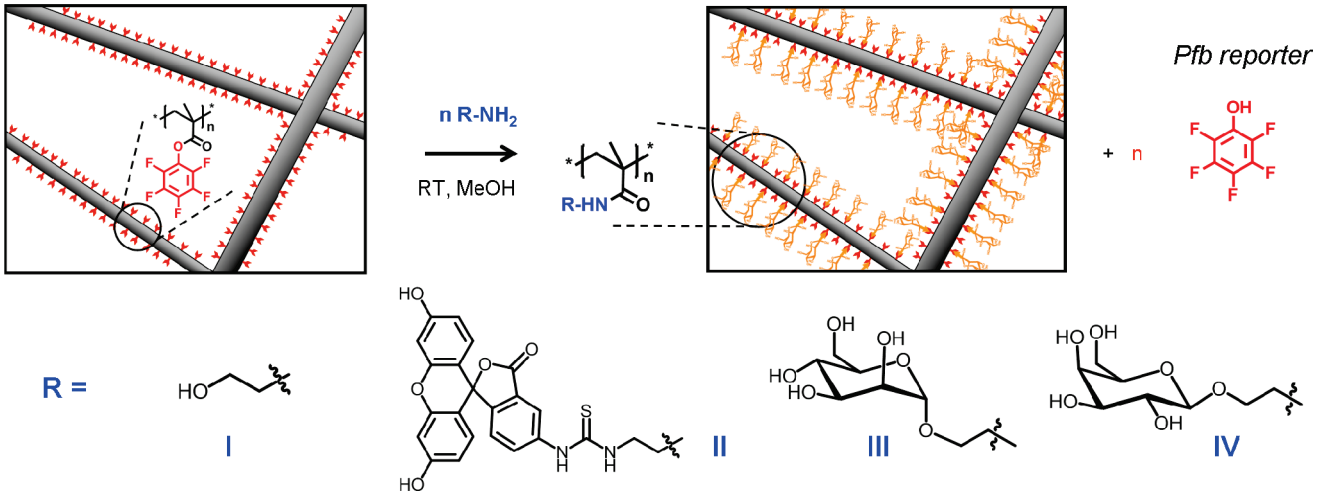

Figure 1. Functionalization of fiber meshes bearing activated esters at the surface allows for the introduction of different amino functional molecules (2-aminoethanol (**I**), aminofluorescein (**II**), 2-aminoethyl-α-D-mannopyranoside (**III**), or β-D-galactopyranoside (**IV**)). Introduction of functional molecules is accompanied by the release of a pentafluorophenol reporter that can be monitored by UV/vis spectroscopy.

been exploited, leading to a clear enrichment of functional biomolecules, e.g., peptides on the fiber surfaces,[22] only a fraction of the biomolecules will be accessible on the fiber surface.

In this respect, the second strategy of postfunctionalization of fiber meshes appears to be more successful.[7,25,28] As functional biomolecules are attached onto the surfaces of preformed fibers, no biomolecules are "wasted" by burying them inside the fiber bulk. The strategy ensures the accessibility of biomolecules and supported biomolecules could even exhibit increased activity compared to solution-based factors.[29]

However, the postfunctionalization strategy often involves multistep procedures such as fiber surface activation (e.g., plasma treatment), linker attachment, activation of the linker, and introduction of the desired biomolecule.[28] For instance, the surface of PCL fibers was activated by plasma treatment, and the resulting carboxylate groups have been activated via carbodiimide chemistry, allowing for gelatin attachment.[25] In another study, fiber nonwovens were made by cospinning of poly(lactide-*co*-glycolide) (PLGA) with PLGA-*block*-PEO-NH_2. The latter introduced an amino group for GRGDY-peptide immobilization using an ethylene glycolbis-(sulfosuccinimidyl succinate) coupling reagent.[26] The layer-by-layer method (LBL) was applied to nylon fibers in order to introduce functional groups.[30]

While functionalization of nanofiber surfaces with proteins or peptides can effectively control cell−material interactions, as adhesion proteins like fibronectin facilitate cell adhesion,[31] monodispersed oligosaccharides have been recognized as highly potent molecules.[32] Carbohydrates are involved in a number of cellular processes like cell communication, proliferation, differentiation, and host−pathogen interactions.[33−35] Carbohydrate structures on pathogens also participate in the induction of host immune response that can be exploited for vaccination.[36,37] One important mechanism by which the immune system senses bacteria is recognition of microorganism-specific saccharide motifs by innate immune receptors. A common receptor−ligand complex is formed between the mammalian Toll-like receptor 4 (TLR4)−MD2−CD14 complex and bacterial lipopolysaccharides (LPS).[38] Host recognition of pathogenic microorganisms induces an immune response by producing antibacterial substances and recruitment of phagocytic cells such as neutrophils or macrophages. Sugars such as mannose-containing oligosaccharides contribute to this process by interacting with macrophages via the mannose receptor, which mediates endocytosis and cytokine production.[39] These are important compounds for signaling cascades to trigger the immune reaction.

The main purpose of the present study was to investigate a one-step spinning process of blends composed of PCL and PPfpMA. By utilizing a single syringe electrospinning setup, nanofiber meshes exhibiting activated Pfp esters on their surfaces could be fabricated, which were prone to directly introduce bioactive molecules such as 2-aminoethyl-α-D-mannopyranoside or 2-aminoethyl-β-D-galactopyranoside leading to nonwovens useful for effective immune stimulation. The reactive meshes have been obtained on a standard electrospin setup by cospinning PCL with a poly(methacrylate) derivative that features pendant-activated esters. The pentafluorophenyl unit is believed to help enrich such ester functionalities on the fiber surface as similar effects have been described and studied for decades occurring in bulk materials and films, but to a lesser extent for submicron-sized fibers.[40−46] The introduction of (bio)functional entities to the fiber surfaces proceeded in a clean manner with amino-functionalized biomolecules. No plasma activation of the fiber meshes and introduction of additional linkers or utilization of activation reagents are required. Conversion and kinetics of the functionalization process were readily monitored by means of UV/vis spectroscopy as the attachment of a functional molecule releases a pentafluorophenol moiety as a detectable unit (cf. Figure 1).

Experimental Section

Materials. Materials used in the bioassays are detailed in the Biological Testing section.

Poly(ethylene oxide) (PEO, M_n = 291 kg/mol, M_w/M_n = 9.83 (gel permeation chromatography, GPC), and M_n = 487 kg/mol, M_w/M_n = 7.52 (GPC)) and poly(methyl methacrylate) (PMMA, M_n = 173 kg/mol, M_w/M_n = 1.88 (GPC)) were purchased from Sigma-Aldrich (Steinheim, Germany) and were used as received. Poly(ε-caprolactone) (PCL) was purchased from Sigma-Aldrich (M_n = 113 kg/mol, M_w/M_n = 1.65 (GPC)); the PCL granulate was dissolved in chloroform, reprecipitated in methanol, and dried in a vacuum at room temperature (PCL used for electrospinning (M_n = 78 kg/mol, M_w/M_n = 1.61 (GPC)). Chloroform ($CHCl_3$, 99.9+%, Merck, Darmstadt, Germany), methanol (MeOH, 99.9+%, Biosolve, Germany), fluorescein-5-isothiocyanate (FITC), tetrahydrofuran (THF), and *N*,*N*-dimethylformamide (DMF), *N*,*N*-dimethylacetamide (DMAc), and 1,2-diaminoethane have been purchased from Sigma-Aldrich (Steinheim, Germany) in 99.9% quality and were used as received. 2-Aminoethanol (AE) (Sigma-Aldrich, Steinheim, Germany) was distilled prior to use. Poly(pentafluorophenyl methacrylate) (PPfpMA, M_n = 29.3 kg/mol, M_w/M_n = 1.67 (GPC)) and poly(*n*-butyl acrylate)

(P*n*BA, M_n = 798 kg/mol, M_w/M_n = 1.77 (GPC)) were synthesized by free radical polymerization as described elsewhere.[47,48] 2-Aminoethylmannoside or galactoside was synthesized following well-documented protocols described elsewhere.[49,50] 99+% purity of the two saccharides was proven by NMR and mass spectrometry.

Preparation of amino-functionalized FITC (II, [2-(aminoethyl)-carbamothioyl]-5-aminofluorescein) and hydroxyl-functionalized FITC (**IIa**, [2-(hydroxyethyl)carbamothioyl]-5-amino fluorescein): A solution of 85.8 μL (1.28 mmol) of 1,2-ethylenediamine in 30 mL of methanol was added dropwise to a solution of 0.5 g (1.28 mmol) of fluorescein-5-isothiocyanate dissolved in 20 mL of methanol. In analogy, 76.9 μL (1.28 mmol) of 2-aminoethanol dissolved in 30 mL of methanol was added dropwise to 0.1 g (0.257 mmol) of FITC dissolved in 20 mL of methanol. Both solutions were stirred for 3 h at room temperature. The solvent was removed under vacuum, and the product was freeze-dried from water to yield 0.56 g (97%) of amino-functionalized and 0.11 g (95%) of hydroxyl-functionalized fluorescein, respectively.

Amino-FITC (**II**). ^{1}H NMR (MeOD) δ (ppm): 3.31 (t, 2H, ^3J = 5.0 Hz, $H_2N-CH_2-CH_2$); 3.98 (t, 2H, ^3J = 5.0 Hz, $H_2N-CH_2-CH_2$); 6.67−6.71 (m, 4H, $Ar^{2,3}$), 6.86−6.90 (m, 2H, $Ar^{2,3}$), 7.24 (d, 1H, ^3J = 8.08 Hz, Ar^1), 7.85 (d, 1H, ^3J = 8.08 Hz, Ar^1), 8.29 (s, 1H, Ar^1).

Hydroxyl-FITC (**IIa**). H NMR (MeOD) δ (ppm): 3.00 (t, 2H, ^3J = 5.1 Hz, $HO-CH_2-CH_2$), 3.66 (t, 2H, ^3J = 5.1 Hz, $HO-CH_2-CH_2$), 6.57−6.67 (m, 4H, $Ar^{2,3}$), 6.82−6.86 (m, 2H, $Ar^{2,3}$), 7.17 (d, 1H, ^3J = 8.32 Hz, Ar^1), 7.77 (d, 1H, ^3J = 8.32 Hz, Ar^1), 8.09 (s, 1H, Ar^1).

Instrumentation. Nuclear magnetic resonance (NMR) spectroscopy measurements were carried out at room temperature using a Bruker DPX-400 spectrometer operating at 400 MHz (^{1}H NMR). As solvent, MeOD (Carl Roth, Karlsruhe, Germany) was used.

Gel permeation chromatography (GPC) measurements with simultaneous UV and RI detection were performed in THF at 25 °C, flow rate 1 mL/min, column settings: two MZ-SDplus columns, 300 × 8 mm (dimensions), 5 μm (particle size), 10^3 and 10^5 Å (porosity). Solutions containing ~0.15 wt % polymer were stirred overnight and filtered through 0.45 μm filters; injected volume was 100 μL. Calibration was done with PLA, PS, or PMMA standards (PSS, Mainz, Germany). In the case of P*n*BA, universal calibration based on linear pS standards (PSS, Germany) was used.

Differential scanning calorimetry (DSC) measurements were performed on a NETZSCH DSC 204 (NETZSCH Gerätebau GmbH, Selb, Germany) under N_2 at a rate of 10 °C/min, and the glass transition temperature was determined from the second heating curve (inflection/peak).

Electrospinning was performed using an apparatus described elsewhere.[52] The setup was composed of a high-voltage power supply (dc, HCP-serie 14-20000, FuG Electronik GmbH, Rosenheim, Germany) and a syringe pump (KD Scientific Inc., Holliston, MA). Plastic 1 mL syringes with disposable blunted tips with nominal inner diameter of 0.584 mm (JG20-2, Howard Electronics, El Dorado, KS) were charged positively, and aluminum foil was used as a collector in a vertical setup. The polymer solution was fed at a rate between 0.2 and 4.7 mL/h by the syringe pump to the blunted needle tip, where a voltage of 5−10 kV was applied. The spinning distance between tip and ground collector was 7 cm. Polymer solutions were freshly prepared by dissolving the polymer overnight via shaking on a shaker (~2 Hz) or mixing with a rock and roll shaker. Solutions of polymer blends were prepared by dissolving both polymers in one pot. Prior to spinning, the blend solution was vigorously agitated either by vortexing or by high-power ultrasound.

For scanning electron microscopy (SEM) measurements using LEO 1550-GEMINI, (Zeiss, Oberkochen, Germany), the resulting fiber meshes were dried, cut into 0.5 × 0.5 cm^2 pieces, and sputtered with Pd/Au. Some of these pieces were set aside for the bioassays. To evaluate the fiber diameter, the software ImageJ (National Institutes of Health, Bethesda, MD) was used.

UV/visible (UV/vis) spectroscopy was performed on a Perkin-Elmer Lambda 2 UV/vis spectral photometer (PerkinElmer, Waltham, MA) at 60 nm min^{-1} in 1 nm intervals. For the pentafluorophenol (Pfp) release studies, Pfp/MeOH solutions with known concentrations were measured with UV/vis spectroscopy. The absorption intensity was plotted at 267 nm against Pfp concentration, and the calibration was conducted using linear regression. The resulting equation was $y = f(c[\mathrm{PFP}]) = 3.7223x$ with correlation coefficients (least-squares method) R^2 = 0.997 96 (Supporting Information Figure S5).

Static contact angles were measured by using a contact angle measuring system G10 from A.KRÜSS Optronic GmbH (Hamburg, Germany). Contact angles were determined by placing a drop of water from a syringe onto the fiber mat and measuring the contact angle within < 10 s of application of the drop. Measurements were done at room temperature. Reported values are averages of three measurements taken at different points on the surface.

X-ray photoelectron spectroscopy (XPS) measurements were done with an Axis 165 instrument (Kratos Analytical, Manchester, UK) with monochromatic Al Kα radiation in hybrid mode, i.e., with electrostatic and with magnetic lenses. The takeoff angle of the emitted electrons was set to 90° related to macroscopic sample surface. Because of the varying surface topography of the samples, the real takeoff angle will differ and therefore the exact information depth will also change in the range from 1 to 10 nm. The size of the measured area (approximately 0.3 × 0.7 mm) led to an average information depth. The charging of the sample during the measurement was compensated with thermal electrons from a filament. A linear background correction was applied, and the high-resolution spectra were fitted with Gaussian functions. The data processing was done with Casa XPS software (Casa Software Ltd., version 2.1.13). In order to delete background signals from the glass slides a correction according to its chemical surface composition was performed.

Biological Testing. Wild-type C57BL/6 mice were housed in the animal facility of the Federal Institute for Risk Assessment (Berlin, Germany). All mice were kept under specific pathogen-free conditions, with food and water *ad libitum*. Mouse peritoneal exudate cells (PECs) were elicited by i.p. injection of 1 mL 4% thioglycollate solution into 8−12-week-old female C57BL/6 mice. After 5 days, mice were sacrificed and PECs were isolated by lavage of the peritoneum with 10 mL ice-cold PBS. Further information for the PECs elicitation and isolation can be found in the literature.[51] Animal experiments were in accordance with local Animal Ethics Committee regulations.

Upon erythrocyte lysis by addition of ammonium chloride, PECs were suspended in Iscove's Modified Dulbecco's Media (IMDM) medium (Gibco Invitrogen, Karlsruhe, Germany). Cell culture medium was supplemented with 10% fetal bovine serum, L-glutamine (2 mM), sodium pyruvate (1 mM), and 1% penicillin/streptomycin. All medium additives were obtained from PAN Biotech, Aidenbach, Germany.

Fibers functionalized with mannose, galactose (specific control), or aminoethanol (unspecific control) with similar dimensions (mat size, mat density, fiber diameter) were placed in the wells of a 96-well plate. Fibers were manually attached to the bottom of the wells of the cell culture plates used. Fibers were not prewet, but no air bubbles could be seen when checking through a light microscope. Subsequently, 2 × 10^5 freshly prepared PECs were seeded in each well and were allowed to adhere to the fiber meshes for 2 h. The attachment was checked by microscope at regular intervals. Nonadherent cells were removed by replacing the medium with prewarmed cell culture medium. Cells were then stimulated by adding the Toll-like receptor-4 (TLR-4) agonist lipopolysaccharide (LPS, Sigma-Aldrich) at a final concentration of 10 ng/mL. Cells were cultivated overnight at 37 °C and 5% CO_2, the culture supernatant was removed from

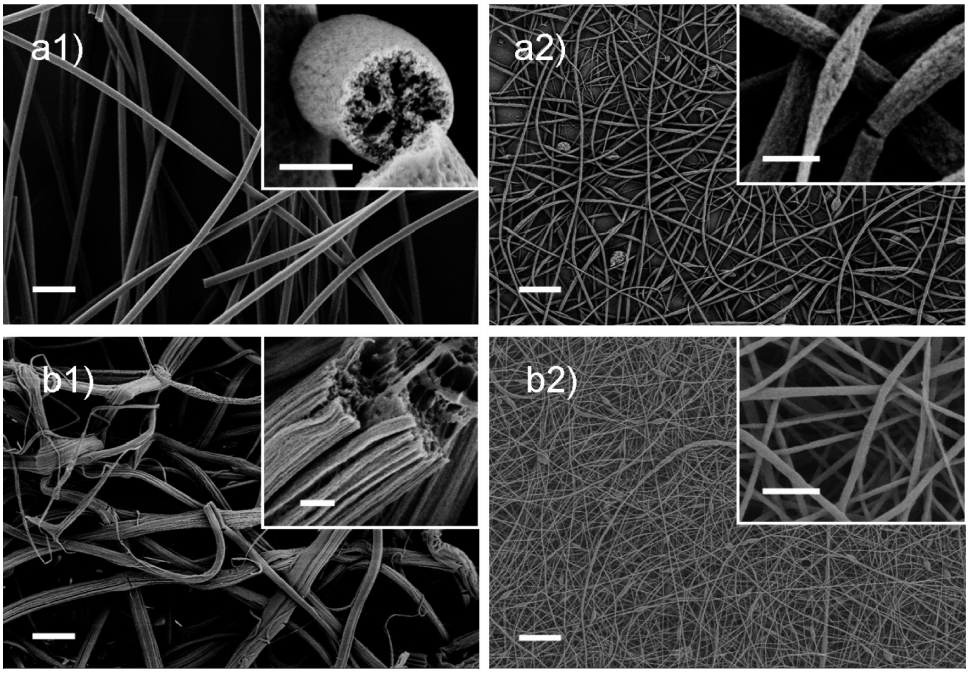

Figure 2. SEM micrographs of meshes obtained by the electrospinning of solutions of pure PPfpMA (a) and PCL/PPfpMA blends (b). The influence of different solvents and changes in concentration were investigated: (a1) 30% w/v, THF/DMF (3:1); (a2, b1, b2) THF/DMF (1:1) (a2) 15.7% w/v, (b1) 22.3% w/v, 12 wt % PCL, (b2) 12.7% w/v, 50.1 wt %; electrospinning conditions: 7 cm tip−collector distance, 0.5−4.7 mL/h, 5−10 kV, 50−64% relative humidity; scale bars = 10 μm, insets: 1 μm.

the cells, and cytokine concentrations were analyzed by enzyme-linked immunosorbent assay (ELISA).

For analysis of cytokine production indirect sandwich ELISA was performed for the quantification of TNF-α. Antibody (Ab) pairs and cytokine standards were purchased from PeproTech (Hamburg, Germany). ELISA was performed according to the manufacturer's instructions. After incubation with the detection antibody, plates were washed three times and incubated with Avidin-HRP (PeproTech) for 30 min at room temperature. ELISA development was performed by using the ABTS substrate (Sigma). Absorbance was measured with an ELISA plate reader (TECAN Infinite M200 NanoQuant, Crailsheim, Germany) at 405 nm (reference wavelength 650 nm).

Statistical analyses were performed with unpaired Student's *t* test. All statistical analyses were performed with the Prism software (Graph Pad Software, San Diego, CA).

Results and Discussion

Fiber Fabrication. To obtain polymer nanofiber meshes with activated ester groups on the fiber surfaces, the electrospinning of poly(pentafluorophenyl methacrylate) (PPfpMA) was investigated. PPfpMA proved to be a highly versatile polymer, exhibiting pendant side-chain activated esters.[47,52,53] PPfpMA can be obtained via controlled radical polymerization techniques (CRP) enabling one to synthesize well-defined copolymers and block copolymers.[47,54] Larger quantities of PPfpMA homopolymer, as required for electrospinning, have been obtained via straightforward free radical polymerization in benzene with azobis(isobutyronitrile) as initiator.[55] The PPfpMA used in this study had an average molecular weight of $M_{n,GPC}$ = 29.3 kg/mol and M_w/M_n = 1.67.

Independent of the rather low molecular weight, pure PPfpMA homopolymer could be successfully electrospun from $CHCl_3$ solutions with 56% w/v polymer to yield polymer fibers with 32 ± 9 μm diameters (cf. Supporting Information Figure S1a). In order to improve the continuity of the process (i.e., to prevent nozzle clogging) and reduce the fiber diameter, the electrospinning process was improved by using less volatile solvents and reducing the polymer concentration (cf. Figure 2a1−a2, Supporting Information Figure S1). Using pure *N,N*-dimethylacetamide (DMAc) as low volatile solvent and a concentration of 20% w/v resulted in the formation of thick porous fibers of 6.8 ± 1.6 μm (Supporting Information Figure S1d). However, nozzle clogging was still observed. Additionally, the obtained fibers showed surface porosity, indicating that solvent evaporation occurred rapidly. It seemed that poor solvent−solute interaction was more dominant than solvent volatility. Therefore, binary solvent mixtures were used, where one solvent was mainly responsible for proper polymer dissolution (e.g., $CHCl_3$, THF). The other component should provide an optimal spinning process, such as DMF, that combines low volatility and conductivity with high polarity.[9] A polymer concentration of 32% w/v and a $CHCl_3$/DMF (3:1 v/v) solvent system resulted in a decrease of fiber diameter to 4.2 ± 1.6 μm. As clogging was still an issue, the concentration was slightly decreased to 30% w/v, while a binary THF/DMF (3:1/v:v) system was used to improve spinning continuity and the fiber morphology. From this, meshes with fiber diameters of 2.0 ± 0.1 μm were spun (Figure 2a1). Interestingly, the fibers presented some porous structuring within the fiber bulk (cf. Figure 2a1, inset), suggesting possible phase separation during the electrospinning process.[56] Another explanation might be craze and crack formation due to an asymmetric drying process after fiber constitution. Cracks might form because remaining DMF in the fiber slowly evaporates from the fiber core. Rapid evaporation at the fiber surface leads to the formation of a solidified polymer skin which prevents the shrinking and hence generates tension in the fiber bulk while slowly drying of the fiber. Spinning continuity was best using a THF/DMF (1:1/v:v) solvent system, which was chosen for further experiments. Reducing the polymer concentration to 17% w/v led to 0.81 ± 0.34 μm sized fibers (cf. Supporting Information Figure S1e). Further decreasing the solute concentration

Table 1. Chemical Composition of Sugar-Modified PCL/PPfpMA Fibers Measured by XPS[a]

samples	C [at. %]	(C_{th})	O [at. %]	(O_{th})	N [at. %]	F [at. %]	(F_{th})
PCL/PPfpMA[b]	62.6	67.1	15.1	18.5	n.d.	22.4	14.4
PPfpMA	57.3	58.8	10.6	11.8	n.d.	32.1	29.4
PCL	83.3	75.0	16.7	25.0	n.d.	n.d.	
mannose	64.4		20.8		n.d.	14.8	
galactose	54.7		30.2		1.5	13.6	

[a] The values were corrected for background signals of the glass slide (uncorrected: cf. Supporting Information Table S1); C 1s spectra of the samples can be seen in Supporting Information Figure S6; n.d. = not detected. [b] PCL/PPfpMA ratio was 1/1 by weight.

to 16% w/v induced partially beaded fibers with fiber diameters of $0.54 \pm 0.29\ \mu$m (cf. Figure 2a2). As a general trend, the nozzle clogging can be prevented by adequate choice of solvent (solvent−solute interaction, volatility) and low polymer loadings.

An interesting feature observed during the process of spinning PPfpMA homopolymer was a significantly increased deposition in the *z*-direction in comparison to the commonly obtained flat meshes (cf. Supporting Information Figure S2). This results in an increase of the mesh thickness and might be of interest for the production of scaffolds that could promote cellular ingrowth[5] by means of the mesh's large porosity.

The increased deposition in the *z*-direction may be attributed to the high humidity as shown by control experiments performed under low humidity conditions. The humidity is supposed to assist the grounding of residual charges from deposited fibers. This prevents repulsion and therefore promotes deposition of additional fibers on the same area, which subsequently leads to thicker meshes.

Pure PPfpMA could be processed effectively by electrospinning into meshes with variable fiber diameters. However, as indicated in Figure 2a1−a2, the resulting meshes were mechanically brittle as indicated by the appearance of a high number of fiber ruptures. This impression was macroscopically confirmed by performing a disassembly experiment, where a mesh was shaken in MeOH. Even a gentle agitation of 1 Hz resulted in a significant mechanical disassembly of the mesh within 12 h. This property is not surprising, considering the low molecular weight of the PPfpMA and the high glass transition temperature (T_g) of = 125 °C, which is close to that of PMMA. Unfortunately, the mechanical instability hampers applicability of the fabrics.

To enhance the mechanical properties of the meshes and render them suitable for applications, the inherent brittleness had to be overcome. For that purpose, PPfpMA was blended with other polymers that improved electrospinning and modulated the mechanical properties of the resulting fibers. PEO, P*n*BA, PMMA, or PCL was utilized to spin binary blend systems with PPfpMA using $CHCl_3$ or THF/DMF as compatibilizing solvents. While the application of high molecular weight P*n*BA, PMMA, or PEO significantly improved both the spinning behavior and the fiber morphology, mat handling did not improve. For a concentration of 12 wt % PCL with respect to the PPfpMA, effective electrospinning was feasible, using a 22.3% w/v polymer solution in THF/DMF (1:1, v:v). The resulting discernible elasticizer effect increased considerably the plastic fracture behavior of the fibers and led to fiber diameters of $2.2 \pm 1.4\ \mu$m (Figure 2b1). In order to further improve this effect, the content of PCL in the blend was increased to ∼50 wt %.

A prepared polymer solution, having ∼12.7% w/v of the polymer blend (PCL/PPfpMA) in THF/DMF (1:1, v:v), appeared moderately turbid even after an intense homogenization step. However, the morphology of the electrospun fiber meshes significantly improved and was close to that of pure PCL mats if spun at comparable conditions resulting in fiber diameters of $0.23 \pm 0.07\ \mu$m (cf. Figure 2b2, Supporting Information Figure S3a,b). It should be noted that the fiber morphology changed when an aged solution was spun without prior homogenization, suggesting that solution demixing should be considered. Moreover, humidity was an important parameter as increased beading occurred during processing under low humidity conditions, which led to less mechanically stable meshes (cf. Supporting Information Figure S3c). Most importantly the obtained electrospun fiber mats at high to moderate humidity could be handled without obvious mechanical disassembly (cf. Figure 2b2). Initial mechanical disassembly experiments proved that a mesh could be agitated at a frequency of ∼2 Hz for 14 days in MeOH without obvious disintegration.

Surface Functionalization of Nonwovens with Diverse Molecules. Electrospinning of a PPfpMA/PCL blend was successful, as the nonwovens met the mechanical robustness required for the application. However, the subsequent functionalization step required the presentation of PPfpMA on the fiber surface, allowing nucleophiles to access the pentafluorophenyl activated esters. X-ray photoelectron spectroscopy (XPS) allowed for the determination of the atomic composition of surfaces, penetrating approximately 1−10 nm into the material. Therefore, XPS is a good tool to investigate the active surface of polymer fiber meshes and determine the fluorine content in organic compounds. Table 1 compares the atom composition of a representative fiber mesh obtained from electrospinning of the PPfpMA/PCL blend solution with control meshes composed of pure PPfpMA or pure PCL. The PPfpMA/PCL fibers contained 22 at. % fluorine (F) on at the surface, confirming the presence of active Pfp esters on the fiber surface. As anticipated, no evidence for F could be found by investigating pure PCL fibers, and a higher content of 32 at. % was evident in the mesh composed of pure PPfpMA. The presence or absence of F could also be demonstrated by evaluating the C 1s spectra of PCL, PPfpMA, or its blend fibers, i.e., from the C−F component (cf. Supporting Information Figure S6). Interestingly, the F content of the PPfpMA/PCL blend fibers appeared to be higher as would be expected for a statistical blend of PCL and PPfpMA in a 1/1 ratio (F vs F_{Th}). The same tendency was observed for pure PPfpMA fibers, however to a lesser extent. The passive localization of the PPfpMA on the surface appeared to be reasonable as enrichment of fluorine compounds at the air−material interface is a well-described phenomenon.[40−46] The effect is highly advantageous because the expensive activated ester component is enriched at the fiber surface where it is accessible. The pure PCL indicated slightly higher C content than the theoretically calculated value, which can be attributed to surface hydrocarbon contaminations.[57]

In order to demonstrate that the surface Pfp-active esters can be accessed and used to introduce functional molecules, meshes of pure PPfpMA and those of PPfpMA/PCL blends were exposed to solutions of 2-aminoethanol (AE) as a simple model substance. The effective functionalization in water/methanol mixtures or methanol can be conveniently monitored following the release of pentafluorophenol (Pfp) by UV/vis spectroscopy at $\lambda = 267$ nm. The liberated c[Pfp] was

Table 2. Model Functionalization Reactions of Fabrics Composed of Either PPfpMA (Homo) or PPfpMA/PCL (Blend) with AE[a]

C [wt %]	time	mass [mg][c]	equiv AE	yield [%]
		Homo		
100	2.5 h	0.7	900	6.3
100	19 h	0.7	900	27.7
100	24 h	6.4	65	16.6
100	24 h[b]	5.2		3.3
		Blend		
88	2 h	2.1	330	4.4
88	6 h	2.1	330	5.0
88	24 h	2.2	315	14.7
88	24 h[b]	2		1.3
48	5.5 h	2.6	490	11.1
48	4 days	2.6	490	50.8
48	5 days	2.6	490	59.8
48	7 days	2.6	490	95.6
50	3 days	9.8	1	2.7
50	4 days	9.8	1	3.5
50	11 days	9.8	1	4.5
50	4 days[b]	8.7		1.4

[a] Functionalization was monitored by UV/vis spectroscopy. [b] Control reaction in MeOH in the absence of the nucleophile. [c] Mass of the meshes concentration (*c*) of PPfpMA in the PPfpMA/PCL blend, equivalence (equiv) AE compared to PPfpMA repeat unit.

assessed based on a calibration curve, which was established prior to the measurement (cf. Experimental Section, Supporting Information Figure S5). Together with the known initial mass of the PPfpMA in the mesh, a reaction yield could be calculated, assuming that quantitative conversion of all active esters is attainable (cf. Table 2). The conversion cannot practically reach 100% as functionalities remain entrapped in the fiber bulk and, hence, cannot participate in the reaction.

The investigated meshes were reacted with AE at room temperature using methanol as the solvent (Table 2). Solutions were gently shaken to enhance homogeneity. The reaction of AE with PPfpMA fiber mats exhibiting an average fiber diameter of 0.81 ± 0.34 μm proceeded well. When 900 equiv excess of AE was used with respect to the activated esters present, the conversion reached ~6% after 2.5 h and ~28% after 19 h. As expected, the decrease of the AE excess to 65 equiv resulted in lower conversions. However, 17% conversion within 24 h indicated substantial functionalization. Control experiments using methanol in the absence of AE revealed about 3% conversion (cf. Table 2 reference). The initial functionalization experiments on nanofiber meshes composed of pure PPfpMA suggested a clean introduction of AE as a sterically straightforward model compound. During the functionalization, the meshes mechanically disintegrated with time, making investigations at longer reaction times problematic and limiting for applications, e.g., for cell studies. However, it should be noted that the integrity of the fiber surface structure was maintained as no dissolution was observed.

Meshes from PCL/PPfpMA blends had improved elasticity and hence were more suitable for potential applications. Nanofiber meshes from PCL/PPfpMA blends with 88, 48, and 50 wt % PPfpMA were exposed to different equivalents of AE. The reaction conditions were preserved as those of the functionalization study of the pure PPfpMA meshes, allowing for the quantification of the conversion by monitoring the Pfp release (Table 2). Using fiber mats with a content of only 12 wt % PPfpMA in the blend, the AE substitution reached ~4% within 2 h and did not dramatically increase over the next 4 h (5%, 6 h). However, after 24 h, the conversion had increased to ~15%. Since this value was ~10 times higher compared to the control reaction, a two-step reaction kinetics was probable. It is likely that the functionalization reaction first proceeded rapidly on easily accessible Pfp-activated esters on the fiber surface, which were converted initially. This functionalization step took place roughly within the first 2 h. As a result, the surface localized Pfp ester groups were transformed to AE-amides that rendered the originally very hydrophobic PPfpMA increasingly hydrophilic. Increased hydrophilicity encouraged surface swelling or partial solubilization and made further Pfp ester groups accessible. However, as observed macroscopically and microscopically by SEM, the fiber integrity was preserved so excessive dissolution can be excluded.

The proposed two-step kinetics had been observed with a variety of other samples, and a long-term experiment confirmed that in principle the entire Pfp-activated esters could be converted, regardless of whether they were hidden in the fiber bulk in the beginning or not. A mesh prepared from a blend of 50 wt % PPfpMA was exposed to 470 equiv of AE (Table 2). After 5.5 h, 11.1% of the theoretical Pfp amount was released. Over the next 4 days the released amount of Pfp increased significantly to ~51% and eventually reached 96% after 7 days. It is noteworthy that the meshes remained mechanically stable and the fiber structures intact.

The functionalization reactions discussed so far utilized large excesses of AE. However, active biomolecules are generally valuable substances that are often present in only a few milligrams. To address this issue, the fiber functionalization procedure was reproduced, investigating reactions with 1 equiv of the nucleophile compared to the Pfp-activated esters. Under these reaction conditions slower kinetics were observed. After 3 days ~3% and after 11 days ~5% of the Pfp moieties had been released. Despite the very slow reaction, conversions were significantly higher when compared to the reference reactions which led to, as an example, 1.4% Pfp hydrolysis within 4 days.

Establishing that the functionalization of fiber meshes is feasible, the spatial uniformity of the functionalization was examined. For this purpose, fluorescein dyes bearing either an amino functionality (**II**) or a hydroxyl functionality (**IIa**) as control were reacted with PPfpMA/PCL fiber meshes. The reaction proceeded in MeOH with 5−8 equiv excess of the dye compared to the Pfp esters. Fluorescence microscopy images of the meshes were taken after 7 and 17 h exposure time to **II** (**IIa** as control). Figure 3a1 shows fluorescent fibers and demonstrates the successful immobilization of the amino-functional fluorescein on the mesh. Dye distribution was highly homogeneous along the fibers in the mesh. The observed fluorescence intensity was superior to that of the mesh that was exposed to the hydroxyl-functionalized fluorescein control (Figure 2b1). The presence of minor fluorescence activity in the control was most likely due to noncovalent adsorption of **IIa** onto hydrophobic fibers. After 17 h, the differences between the functionalization reaction and the control became even more obvious as depicted in Figure 3 (a2 vs b2). A quatitative comparison of the fluorescence intensity of the meshes after 17 h with that after 2 h is difficult. Because of a strong increase in fluorescence intensity, a decrease in gain and exposure time of the fluorescence microscope was required. The results correlated to the UV/vis spectroscopy investigation discussed above and suggested a clean and homogeneous introduction of functional molecules to the surface of PPfpMA/PCL fiber meshes. This also implies a homogeneous distribution of PPfpMA on the fiber surface within the lateral resolution of optical microscopy. Furthermore, the obvious change in polarity during functionalization of the hydrophobic PPfpMA/PCL fibers was confirmed

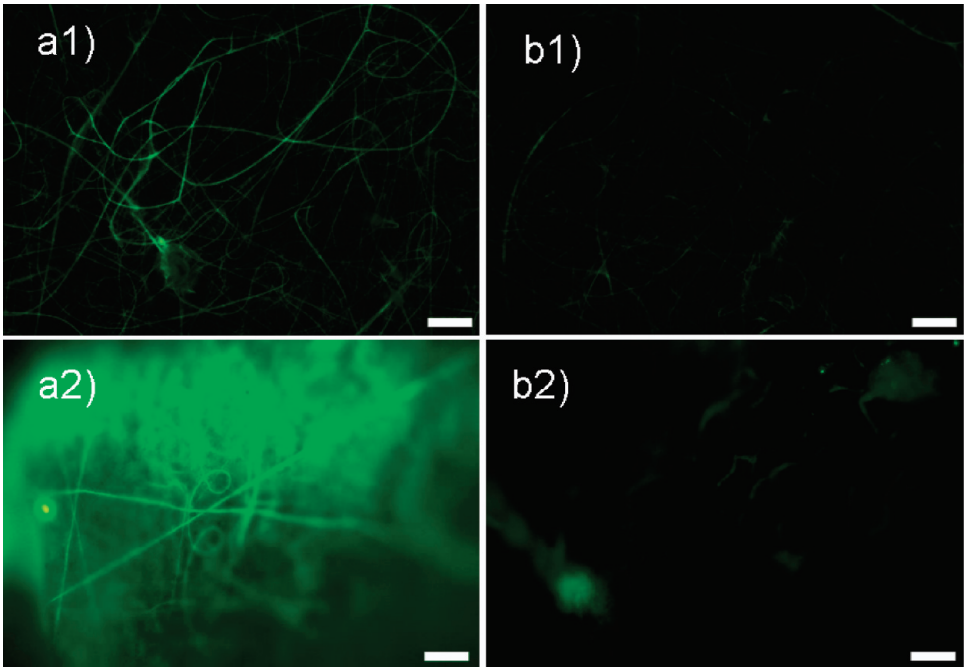

Figure 3. Reaction of aminofluorescein (**II**, a1, a2) or hydroxyfluorescein (**IIa**, b1, b2) with PCL/PPfpMA fiber meshes after 7 h (a1/b1) and 17 h (a2/b2) suggests a homogeneous distribution of the dye as depicted from the fluorescence light micrographs. Reaction conditions: (a) 5 equiv **II** vs Pfp, (b) 8 equiv **IIa** vs Pfp; microscope settings: a1/b1: 7.9× gain, 473.1 ms, a2/b2: 5.6× gain, 250.9 ms, scale bars = 10 μm.

by contact angle measurements. As expected, an increase in the hydrophilicity of the meshes resulted in a decrease of the static contact angle from 138° to 0° after 14-day reaction time with AE. As the contact angle measurement of nanostructured, irregular fiber meshes is complicated, only static contact angle and qualitative interpretation of the results is possible. Together with the UV studies and fluorescence microscopy data, the reactive fiber meshes were considered to be suitable for further functionalization with biologically active saccharide molecules.

Surface Functionalization with Bioactive Molecules. Electrospun nonwovens from PPfpMA/PCL blends were functionalized with mannose (**III**) or galactose (**IV**) containing a terminal amine (cf. Figure 1) to study the activation of cytokine production of macrophages by these meshes. Both saccharides were synthesized according to protocols reported previously.[49,50] PPfpMA/PCL meshes that exhibit Pfp-activated ester groups on their surfaces were exposed to methanolic solutions of the two saccharides **III** and **IV**. Pfp release was monitored by UV/vis spectroscopy. The functionalization proceeded slowly due to a low excess of amino sugars of ~5 equiv with respect to the Pfp ester moieties in the fibers. For mannose, ~3% conversion was found after 15 h and ~4% after 9 days. The functionalization with galactose was slower in the beginning (2% after 15 h) but reached a degree of ~6% within 8 days. The low conversions can be attributed to both the small excesses and the bulky nature of the saccharide entities. However, both conversion values were still significantly higher than the control experiments, suggesting a faster reaction of the amino sugars with the activated ester compared to methanolysis (~1.4% after 4 days). The probability of a reaction of amino functional sugars with the esters of the PCL leading to an ester amination might be given and useful. However, considering the differences in reactivity between the ester and the Pfp esters, the enrichment of the Pfp esters on the fiber surfaces as well as the bulkiness and low excess of the monosaccharide entities, a specific reaction with the Pfp esters is rather likely.

In order to ensure the immobilization of the saccharides onto the fiber surface, XPS was used to characterize the elemental surface composition quantitatively (cf. Table 1). Comparing the composition of the pure PCL/PPfpMA mesh with those of the mats after reaction with mannose or galactose indicated a decrease of the corresponding fluorine content from 22 at. % F to 14−15 at. % F. These findings confirmed the UV/vis data supporting the release of the Pfp moieties and suggested effective functionalization. In addition, for galactose functionalized fibers the nitrogen atom from the linker unit can be detected as well. This observation coincided with the findings from the UV spectroscopy that galactose seemed to be immobilized to a higher extent than mannose. Furthermore, from the C 1s spectra a decrease of the C−F component and an increase of C−O component were found, supporting the release of Pfp and binding of the sugar moieties (Supporting Information Figure S6d). However, it should be noted that the partially solvated and therefore dynamic nature of the surface layer of these fibers prevented the accurate interpretation of changes in C:O:N composition due to surface reconstitution events that might take place during drying. In addition, the determination of absolute/true surface composition on not-flat polymeric substrates exhibiting compositional gradients is not trivial. The change of surface composition on these surfaces measured with XPS is therefore regarded more qualitatively. Moreover, it should be noted that XPS gave an average composition value over a depth down to 1−10 nm depending on the exact angle of the detector unit to the sample surface. This implies that also nonaccessible regions are detected, making a fluorine content decrease of about 30−40 at. % already significant.

The mesh characterizations by means of XPS and UV/vis spectroscopy confirmed an effective functionalization and introduction of functional saccharides onto the fiber surface. However, proof of the introduction and accessibility of functional saccharide entities could be provided by testing responses of an appropriate biological system. For this purpose,

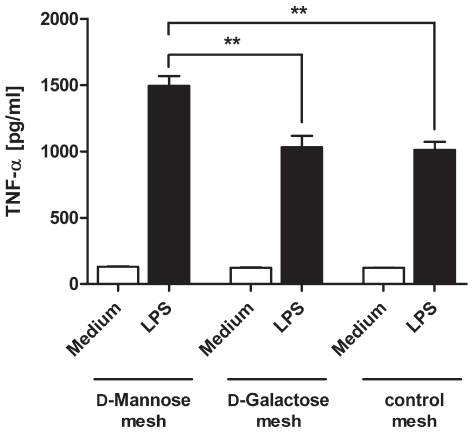

Figure 4. TNF-α production by peritoneal exudate cells (PEC) after stimulation with LPS in combination with the functionalized meshes. PECs were seeded on the meshes and stimulated in the presence (black bars) or absence (white bars) of 10 ng/mL LPS overnight. TNF-α was measured in supernatants of stimulated macrophages. Measurements were performed in triplicates. Data are expressed as mean ± standard error of mean. Significance was tested with the one-tailed unpaired Student's *t* test (**: $p < 0.01$).

initial bioassays were performed investigating the activation of macrophages on galactose- or mannose-functionalized meshes as well as on aminoethanol-functionalized control meshes.

Biological Testing. Certain carbohydrates are recognized by lectins of the immune system, which are expressed on the surface of immune cells such as antigen-presenting cells (APCs), e.g., macrophages.[36] In particular, mannose-rich glycans of a number of pathogens were reported to be recognized by C-type lectin receptors such as the mannose receptor, DC-SIGN, or murine DC-SIGN homologues.[58,59] Thus, mannose-functionalized fiber meshes were investigated to elucidate whether lipopolysaccharide-mediated stimulation of APCs could be enhanced. Pro-inflammatory cytokines released by APCs upon stimulation such as tumor necrosis factor-alpha (TNF-α) were measured as readout parameters to monitor stimulation of inflammatory pathways. As negative control, aminoethanol-functionalized meshes were included in the study, whereas galactose-functionalized meshes served as specificity control.

To analyze whether macrophage cultivation on the fiber meshes increased cytokine production, freshly prepared mouse peritoneal exudate cells (PECs) consisting mainly of peritoneal macrophages were seeded on the meshes and were stimulated with lipopolysaccharide (LPS) overnight. The meshes alone did not induce the production of TNF-α by macrophages (Figure 4). LPS is found in the outer membrane of Gram-negative bacteria and induces cytokine production in antigen-presenting cells through stimulation of the Toll-like receptor (TLR)-4 signaling pathway.[38] PEC stimulation in the presence of LPS induced a marked production of TNF-α. However, in the presence of the mannose-functionalized fiber mesh the production of TNF-α was significantly increased (Figure 4).

The results indicate that stimulation with the plate-bound mannose-functionalized fibers in the presence of LPS had a synergistic effect in that TNF-α production was increased. This finding indicates that the sugar-functionalized fibers are functional and that functionality is surface accessible. The AE- and galactose-functionalized fiber meshes show a significantly lower (~30%) activation under comparable conditions, which proved that the increase in TNF-α production upon mannose fiber stimulation is indeed specific. It is also in line with previous publications where murine macrophages were efficiently targeted by mannosylated proteins such as mannosylated bovine serum albumin.[60−62] For the human C-type lectin receptor (DC-SIGN), mannose-dependent enhancement of TLR-4 induced cytokine production has been proven.[59] There are five mouse homologues of the human DC-SIGN molecule, of which particularly SIGN-R1 and SIGN-R3 bind to mannose-rich structures.[63] In conclusion, the increased effect of LPS/mannose meshes on macrophage cytokine production in this study is most likely due to the engagement of either the mannose receptor or DC-SIGN homologues. The mannosylated fiber meshes are a proof-of-concept, and fiber meshes decorated with more complex oligosaccharide structures are expected to be even more specific in modulating signaling pathways in the immune system.

Conclusion

In summary, reactive fiber meshes based on Pfp activated esters were successfully fabricated and functionalized with model substances and saccharides. Pure PPfpMA fiber fabrics were successfully electrospun; for further use, PCL/PPfpMA blends were cospun to improve the handling of the mat and the fiber morphology verified by SEM. UV/vis spectroscopy demonstrated a clean reaction with 2-aminoethanol that was supported by the increased hydrophilicity of the mats from contact angle measurements. The homogeneous distribution of PPfpMA within the blend was suggested by its reaction with amino-functional fluorescein as shown by fluorescence microscopy of the reacted mats. This fiber mesh is a versatile platform for simple immobilization of biomolecules as shown for two sugar molecules. PPfpMA/PCL fibers were functionalized with either mannose or galactose as indicated by UV/vis spectroscopy and XPS. Sugar-functionalized fiber meshes triggered specific interactions with biological systems. Future work will utilize complex sugars for different biological applications.

Acknowledgment. We thank M. Antonietti, K. T. Wiss, U. Vogel, D. Grünstein, and A. Holländer for their contributions to the project. Funding was provided by the joint program of Max Planck Society & Fraunhofer Society (MPG-FhG project on bioactive surfaces), Henkel (Chimera for industries), the U.S. Department of Commerce through the National Textiles Center (US-NTC), and the German Federal Ministry of Education and Research (BMBF).

Supporting Information Available: Additional SEM images of pure PPfpMA and PCL/PPfpMA fibers, Pfp calibration curve for UV/vis spectroscopy, XPS C 1s spectra, and raw XPS composition. This material is available free of charge via the Internet at http://pubs.acs.org.

References and Notes

(1) Stevens, M. M.; George, J. H. *Science* **2005**, *310*, 1135–1138.
(2) Langer, R.; Tirrell, D. A. *Nature* **2004**, *428*, 487–492.
(3) Hutmacher, D. W. *J. Biomater. Sci., Polym. Ed.* **2001**, *12*, 107–124.
(4) Vogel, V.; Baneyx, G. *Annu. Rev. Biomed. Eng.* **2003**, *5*, 441–463.
(5) Gentsch, R.; Börner, H. G. *Adv. Polym. Sci.* **2010**, DOI: 10.1007/12_2010_80.
(6) Lutolf, M. P.; Hubbell, J. A. *Nature Biotechnol.* **2005**, *23*, 47–55.
(7) Liang, D.; Hsiao, B. S.; Chu, B. *Adv. Drug Delivery Rev.* **2007**, *59*, 1392–1412.
(8) Greiner, A.; Wendorff, J. H. *Angew. Chem., Int. Ed.* **2007**, *46*, 5670–5703.
(9) Ramakrishna, S.; Fujihara, K.; Teo, W.-E.; Lim, T.-C.; Ma, Z. *An Introduction to Electrospinning and Nanofibers*; World Scientific Publishing Co. Pvt. Ltd.: Singapore, 2005; p 275.
(10) Teo, W.-E.; He, W.; Ramakrishna, S. *Biotechnol. J.* **2006**, *1*, 918–929.
(11) Li, D.; Xia, Y. *Adv. Mater.* **2004**, *16*, 1151–1170.

(12) Gentsch, R.; Boysen, B.; Lankenau, A.; Börner, H. G. *Macromol. Rapid Commun*. **2010**, *31*, 59–64.
(13) Schindler, M.; Ahmed, I.; Kamal, J.; Nur-E-Kamal, A.; Grafe, T. H.; Chung, H. Y.; Meiners, S. *Biomaterials* **2005**, *26*, 5624–5631.
(14) Boudriot, U.; Dersch, R.; Greiner, A.; Wendorff, J. H. *Artif. Organs* **2006**, *30*, 785–792.
(15) Kwon, I. K.; Kidoaki, S.; Matsuda, T. *Biomaterials* **2005**, *26*, 3929–3939.
(16) Xu, C. Y.; Yang, F.; Wang, S.; Ramakrishna, S. *J. Biomed. Mater. Res., Part A* **2004**, *71A*, 154–161.
(17) Curtis, A.; Wilkinson, C.; Curtis, A.; Wilkinson, C. *Mater. Today* **2001**, *4*, 22–28.
(18) Chen, C. S.; Mrksich, M.; Huang, S.; Whitesides, G. M.; Ingber, D. E. *Science* **1997**, *276*, 1425–1428.
(19) Spatz, J. P.; Geiger, B. Molecular engineering of cellular environments: Cell adhesion to nano-digital surfaces. In *Cell Mechanics*: Elsevier Academic Press Inc.: San Diego, 2007; 83, 89.
(20) Silva, G. A.; Czeisler, C.; Niece, K. L.; Beniash, E.; Harrington, D. A.; Kessler, J. A.; Stupp, S. I. *Science* **2004**, *303*, 1352–1355.
(21) Yang, Q.; Wu, J.; Li, J. J.; Hu, M. X.; Xu, Z. K. *Macromol. Rapid Commun*. **2006**, *27*, 1942–1948.
(22) Sun, X. Y.; Shankar, R.; Börner, H. G.; Ghosh, T. K.; Spontak, R. J. *Adv. Mater*. **2007**, *19*, 87–91.
(23) Sun, Z. C.; Zussman, E.; Yarin, A. L.; Wendorff, J. H.; Greiner, A. *Adv. Mater*. **2003**, *15*, 1929–1932.
(24) Sun, X. Y.; Nobles, L. R.; Börner, H. G.; Spontak, R. J. *Macromol. Rapid Commun*. **2008**, *29*, 1455–1460.
(25) Ma, Z. W.; He, W.; Yong, T.; Ramakrishna, S. *Tissue Eng*. **2005**, *11*, 1149–1158.
(26) Kim, T. G.; Park, T. G. *Tissue Eng*. **2006**, *12*, 221–233.
(27) Ekaputra, A. K.; Prestwich, G. D.; Cool, S. M.; Hutmacher, D. W. *Biomacromolecules* **2008**, *9*, 2097–2103.
(28) Yoo, H. S.; Kim, T. G.; Park, T. G. *Adv. Drug Delivery Rev*. **2009**, *61*, 1033–1042.
(29) Patel, S.; Kurpinski, K.; Quigley, R.; Gao, H. F.; Hsiao, B. S.; Poo, M. M.; Li, S. *Nano Lett*. **2007**, *7*, 2122–2128.
(30) Krogman, K. C.; Lowery, J. L.; Zacharia, N. S.; Rutledge, G. C.; Hammond, P. T. *Nature Mater*. **2009**, *8*, 512–518.
(31) Ruoslahti, E. *Annu. Rev. Biochem*. **1988**, *57*, 375–413.
(32) Plante, O. J.; Palmacci, E. R.; Seeberger, P. H. *Science* **2001**, *291*, 1523–1527.
(33) Seeberger, P. H.; Werz, D. B. *Nat. Rev. Drug Discovery* **2005**, *4*, 751–763.
(34) Liang, P. H.; Wu, C. Y.; Greenberg, W. A.; Wong, C. H. *Curr. Opin. Chem. Biol*. **2008**, *12*, 86–92.
(35) Kinjo, Y.; Wu, D.; Kim, G. S.; Xing, G. W.; Poles, M. A.; Ho, D. D.; Tsuji, M.; Kawahara, K.; Wong, C. H.; Kronenberg, M. *Nature* **2005**, *434*, 520–525.
(36) Lepenies, B.; Seeberger, P. H. *Immunopharmacol. Immunotoxicol*. **2010**, *32*, 196–207.
(37) Lepenies, B.; Yin, J.; Seeberger, P. H. *Curr. Opin. Chem. Biol*. **2010**, *14*, 404–411.
(38) Miller, S. I.; Ernst, R. K.; Bader, M. W. *Nat. Rev. Microbiol*. **2005**, *3*, 36–46.
(39) Taylor, M. E.; Conary, J. T.; Lennartz, M. R.; Stahl, P. D.; Drickamer, K. *J. Biol. Chem*. **1990**, *265*, 12156–12162.
(40) Thomas, R. R.; Anton, D. R.; Graham, W. F.; Darmon, M. J.; Sauer, B. B.; Stika, K. M.; Swartzfager, D. G. *Macromolecules* **1997**, *30*, 2883–2890.
(41) Elman, J. F.; Johs, B. D.; Long, T. E.; Koberstein, J. T. *Macromolecules* **1994**, *27*, 5341–5349.
(42) Affrossman, S.; Bertrand, P.; Hartshorne, M.; Kiff, T.; Leonard, D.; Pethrick, R. A.; Richards, R. W. *Macromolecules* **1996**, *29*, 5432–5437.
(43) McLain, S. J.; Sauer, B. B.; Firment, L. E. *Macromolecules* **1996**, *29*, 8211–8219.
(44) Schaub, T. F.; Kellogg, G. J.; Mayes, A. M.; Kulasekere, R.; Ankner, J. F.; Kaiser, H. *Macromolecules* **1996**, *29*, 3982–3990.
(45) Deitzel, J. M.; Kosik, W.; McKnight, S. H.; Tan, N. C. B.; DeSimone, J. M.; Crette, S. *Polymer* **2002**, *43*, 1025–1029.
(46) Hunley, M. T.; Harber, A.; Orlicki, J. A.; Rawlett, A. M.; Long, T. E. *Langmuir* **2008**, *24*, 654–657.
(47) Eberhardt, M.; Theato, P. *Macromol. Rapid Commun*. **2005**, *26*, 1488–1493.
(48) Hentschel, J.; Börner, H. G. *Macromol. Biosci*. **2009**, *9*, 187–194.
(49) Chernyak, A. Y.; Sharma, G. V. M.; Kononov, L. O.; Krishna, P. R.; Levinsky, A. B.; Kochetkov, N. K.; Rao, A. V. R. *Carbohydr. Res*. **1992**, *223*, 303–309.
(50) Ni, J.; Singh, S.; Wang, L.-X. *Bioconjugate Chem*. **2003**, *14*, 232–238.
(51) Coligan, J. E. *Short Protocols in Immunology: A Compendium of Methods from Current Protocols in Immunology*; John Wiley & Sons: Hoboken, NJ, 2005.
(52) Tahir, M. N.; Eberhardt, M.; Theato, P.; Faiss, S.; Janshoff, A.; Gorelik, T.; Kolb, U.; Tremel, W. *Angew. Chem., Int. Ed*. **2006**, *45*, 908–912.
(53) Theato, P. *J. Polym. Sci., Part A: Polym. Chem*. **2008**, *46*, 6677–6687.
(54) Matyjaszewski, K.; Xia, J. H. *Chem. Rev*. **2001**, *101*, 2921–2990.
(55) Eberhardt, M.; Mruk, R.; Zentel, R.; Theato, P. *Eur. Polym. J*. **2005**, *41*, 1569–1575.
(56) Bognitzki, M.; Czado, W.; Frese, T.; Schaper, A.; Hellwig, M.; Steinhart, M.; Greiner, A.; Wendorff, J. H. *Adv. Mater*. **2001**, *13*, 70–72.
(57) Kasemo, B.; Lausmaa, J. *J. Biomed. Mater. Res., Part B* **1988**, *22*, 145–158.
(58) Boonyarattanakalin, S.; Liu, X. Y.; Michieletti, M.; Lepenies, B.; Seeberger, P. H. *J. Am. Chem. Soc*. **2008**, *130*, 16791–16799.
(59) Gringhuis, S. I.; den Dunnen, J.; Litjens, M.; van der Vlist, M.; Geijtenbeek, T. B. H. *Nature Immunol*. **2009**, *10*, 1081–1088.
(60) Takata, I.; Chida, K.; Gordon, M. R.; Myrvik, Q. N.; Ricardo, M. J.; Kucera, L. S. *J. Leukoc. Biol*. **1987**, *41*, 248–256.
(61) Shimizu, Y.; Takagi, H.; Nakayama, T.; Yamakami, K.; Tadakuma, T.; Yokoyama, N.; Kojima, N. *Parasite Immunol*. **2007**, *29*, 229–239.
(62) Un, K.; Kawakami, S.; Suzuki, R.; Maruyama, K.; Yamashita, F.; Hashida, M. *Hum. Gene Ther*. **2010**, *21*, 65–74.
(63) Galustian, C.; Park, C. G.; Chai, W. G.; Kiso, M.; Bruening, S. A.; Kang, Y. S.; Steinman, R. M.; Feizi, T. *Int. Immunol*. **2004**, *16*, 853–866.